Fossil organic carbon utilization in marine Arctic fjord sediments by subsurface micro-organisms

Manuel Ruben [1,2] ✉, Jens Hefter [1], Florence Schubotz [2,3], Walter Geibert [1], Martin Butzin [1,3], Torben Gentz [1], Hendrik Grotheer [1,3], Matthias Forwick [4], Witold Szczuciński [5] & Gesine Mollenhauer [1,2,3] ✉

Rock-derived or petrogenic organic carbon has traditionally been regarded as being non-bioavailable and bypassing the active carbon cycle when eroded. However, it has become apparent that this organic carbon might not be so inert, especially in fjord systems where petrogenic organic carbon influxes can be high, making its degradation another potential source of greenhouse gas emissions. The extent to which subsurface micro-organisms use this organic carbon is not well constrained, despite its potential impacts on global carbon cycling. Here, we performed compound-specific radiocarbon analyses on intact polar lipid–fatty acids of live micro-organisms from marine sediments in Hornsund Fjord, Svalbard. By this means, we estimate that local bacterial communities utilize between $5 \pm 2\%$ and $55 \pm 6\%$ (average of $25 \pm 16\%$) of petrogenic organic carbon for their biosynthesis, providing evidence for the important role of petrogenic organic carbon as a substrate after sediment redeposition. We hypothesize that the lack of sufficient recently synthesized organic carbon from primary production forces micro-organisms into utilization of petrogenic organic carbon as an alternative energy source. The input of petrogenic organic carbon to marine sediments and subsequent utilization by subsurface micro-organisms represents a natural source of fossil greenhouse gas emissions over geological timescales.

Shales and other sedimentary deposits store around 90% of global organic carbon (OC)[1]. However, this fossil rock-derived or petrogenic OC (OC_{petro}) has been widely neglected as a potential microbial substrate and source of fossil greenhouse gases[2] (GHGs). Traditionally, OC_{petro} has not been included in studies of the active carbon cycle as the majority of it was synthesized, deposited and degraded millions of years ago and is commonly regarded as non-bioavailable[2]. However, within the past two decades, several studies have investigated the availability of OC_{petro} from different sources as a substrate for micro-organisms, painting a more diverse picture of its bioavailability[2-6]. Globally, OC_{petro} oxidation is estimated to account for release of 40–100×10^6 tC annually[7], opposing the effects of OC burial[8] and silicate weathering[9]. Thus, a proper assessment of OC_{petro} bioavailability and the role of micro-organisms becomes increasingly important as more evidence of GHG release from OC_{petro} into the atmosphere is discovered[6,10–13].

Previous work focused on dissolved OC from glacial runoff, showing it to be highly bioavailable, despite its old age[14,15]. Although microbial communities may play a crucial role in glacial nutrient and carbon

[1]Alfred Wegener Institut, Helmholtz Centre for Polar- and Marine-Research, Bremerhaven, Germany. [2]University of Bremen, Bremen, Germany. [3]MARUM - Center for Marine Environmental Sciences, University of Bremen, Bremen, Germany. [4]Department of Geosciences, UiT The Arctic University of Norway, Tromsø, Norway. [5]Geohazards Research Unit, Institute of Geology, Adam Mickiewicz University, Poznań, Poland. ✉e-mail: manuel.ruben@awi.de; Gesine.mollenhauer@awi.de
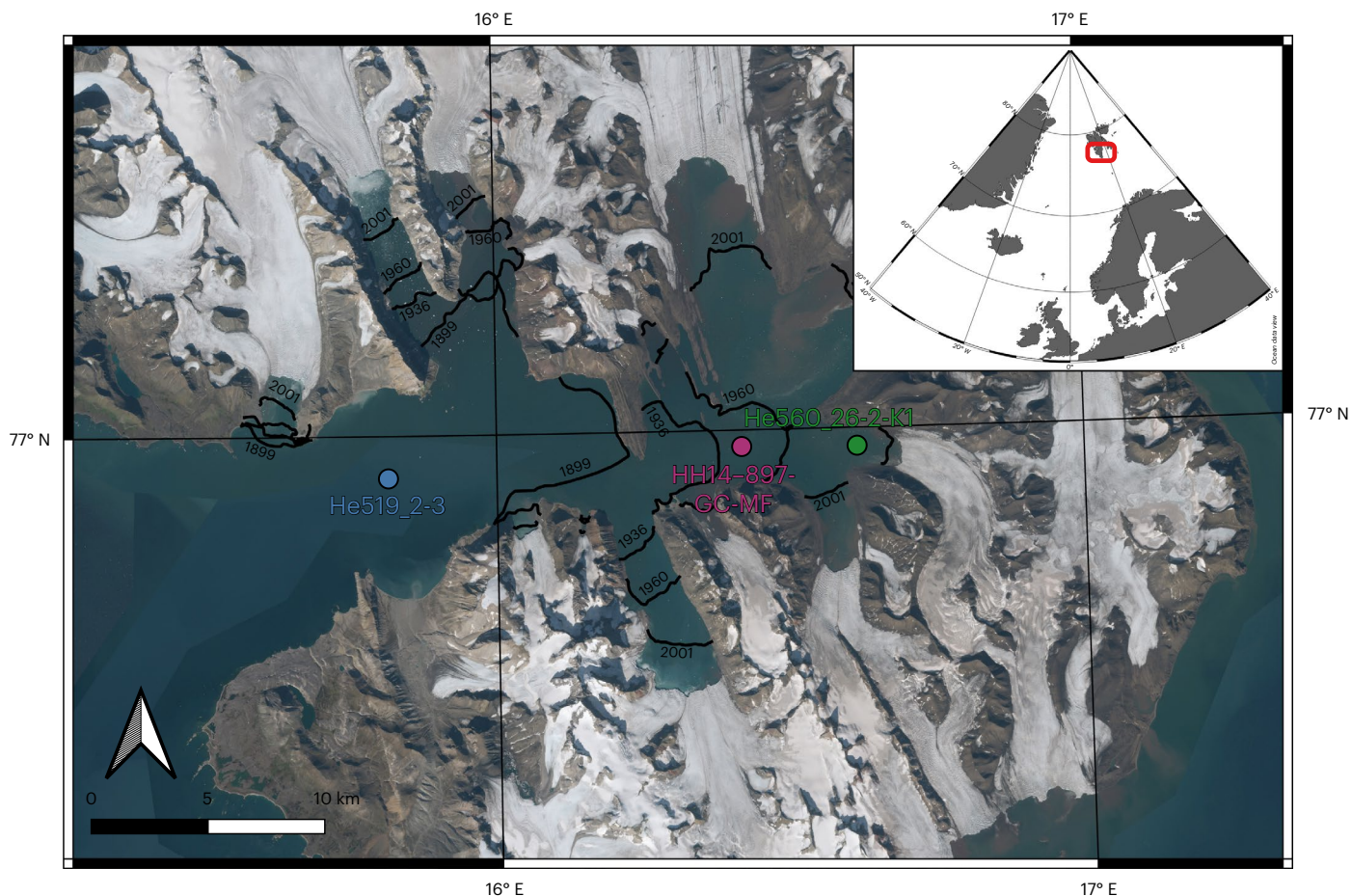
Fig. 1 | Map of Hornsund Fjord in Svalbard with core locations. Core locations with respect to reconstructed retreating glacier termini lines in black of the years 1899, 1936, 1960 and 2001 (modified after ref. 27). The location of marine-influenced main basin short core He519_2-3 is shown in blue, that of central Brepollen long core HH14-897-GC-MF in purple and that of glacier termini core He560_26-2-K1 in green. The map was extracted from a satellite imagery mosaic prepared by the Norwegian Polar Institute, based on Copernicus Sentinel data 2020.

cycling[16], the extent to which the particulate OC supplied by glaciers can be utilized by micro-organisms after its redeposition is virtually unexplored. According to conservative estimates, fjords bury about 18 Mt of OC annually (~11% of marine carbon burial)[17]. Globally, about 11% of landmasses are covered by polar ice sheets and alpine glaciers[18], eroding into the underlying bedrocks[19], including OC-rich strata. Increasing temperatures at high latitudes[20] are expected to increase runoff and sediment exported from both polar glaciers[21] and ice sheets[22] to downstream depositional environments, thus increasing OC_{petro} fluxes in the upcoming decades[23]. At marine-terminating glaciers, the bulk of this OC_{petro} is deposited within a distance of several kilometres from glacier termini[24], with a strong dominance of particulate OC over dissolved OC exported from ice sheets[25]. However, OC_{petro} deposition is not limited to fjords but may supply 40–50% of OC buried in Arctic Ocean sediments[26]. It is therefore of interest whether this vast pool of remobilized OC_{petro} can be microbially degraded, and a proper budget and assessment of its rates are necessary to understand impacts on the global carbon cycle.

OC dynamics in Hornsund Fjord

To investigate this process, we analysed three sediment cores, two short and one long, from Hornsund Fjord, Svalbard (Fig. 1). Hornsund's marine-influenced main basin is separated from the tidewater-glacier-dominated inner basin, Brepollen, by a shallow sill. The Brepollen basin was formed during the last century following the post Little Ice Age deglaciation[27]. The most marine-influenced

core (27-cm-long core He519_2-3) was retrieved from the centre of the main basin at a depth of 202 m. It records the sedimentary history from approximately the 1950s to 2018. A gravity core was collected in the Brepollen basin centre (149-cm-long core HH14-897-GC-MF) at a water depth of 140 m, archiving the time span from the 1960s to 2014. The 23-cm-long core, He560_26-2-K1, was taken ~1 km from the glacier termini at a water depth of 46 m, covering the time period from about 2012 to 2020 (Methods).

The catchment geology of the Hornsund Fjord is very diverse[28]. The majority of sediments supplied to the fjord come from the eastern part of the drainage basin, built of OC-rich Palaeogene mudstones and sandstones formed in a continental shelf sea environment (Supplementary Information)[28,29]. The area is mainly glacier-covered[27]; however, these strata extend northwards. The better exposure displays some low- to mid-grade coal seams; however, these represent only a minor portion of the rock volume[30] (<170-m-thick unit)[31]. Since the late nineteenth century, the local glaciers have been retreating rapidly at rates of several tens of metres to more than 100 m annually[27], simultaneously shifting the sedimentary depocentre alongside the glacier termini position[32]. Sediment accumulation rates in the studied core locations varied from more than 10 cm to a few millimetres per year with respect to distance from the retreating glacier termini. Average total OC (TOC) contents range between 1.3 ± 0.1 and 1.9 ± 0.1 wt% (mean ± s.d.) and are constant throughout the individual cores, independent of glacial proximity (Fig. 2a). The origin of the OC was assessed using several geochemical parameters and biomarker indices, including bulk $\delta^{13}C$,
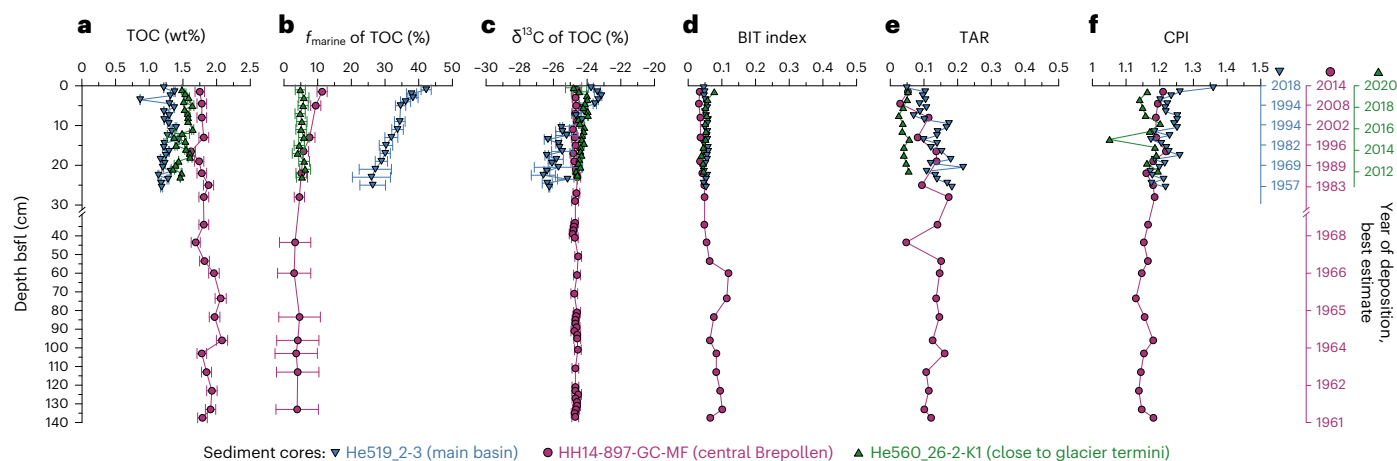
Fig. 2 | Bulk organic matter parameters and biomarker indices plotted against depth and year of deposition. a–f, TOC content (**a**), contribution of marine OC to TOC (f_{marine}; **b**), stable carbon isotope composition of OC (δ^{13}C; **c**), BIT index (**d**), TAR (**e**) and CPI (**f**) for the three analysed sediment cores. Data are presented as mean values. Given uncertainties in **a** and **c** are based on standard deviations of duplicate measurements of each sample; uncertainties in **b** display propagated 1σ errors from bulk radiocarbon measurements, sediment age model and surface DIC age model (Methods). The deposition years are best estimates of the sediment age models (uncertainties and details in Supplementary Information).

fatty-acid-based terrestrial aquatic ratio (TAR)[33], the branched and isoprenoid tetraether (BIT) index as a soil OC marker[34], the n-alkane carbon preference index (CPI) as an indicator for degradation/thermal maturity[35] (Fig. 2c–f and Methods) and bulk radiocarbon (F^{14}C) signature (Fig. 3b,d,f). Contributions to the OC pool by terrestrial plants and soils can be neglected based on both the low TAR and BIT index, which reflect exclusive input of fresh, soil-derived organic matter and are not sensitive to old, mature terrestrial OC from source rock[34]. Based on the above-mentioned biogeochemical parameters, all three cores show a homogenous OC composition consisting of a mixture of two types of material: (1) young, freshly synthesized, labile marine organic matter (OC_{marine}) from primary production; and (2) old, thermally very mature, supposedly non-bioavailable OC_{petro} eroded from organic-rich sedimentary rocks in the fjord catchment[29]. Further evidence for a petrogenic origin of much of the organic matter is provided by the infinite compound-specific radiocarbon ages of long-chain n-alkanes extracted from the central Brepollen core (Supplementary Table 1). Even though primary production rates in Hornsund are similar[36] to other fjord systems with marine-terminating glaciers[37], the relative abundance of sedimentary OC_{marine} (f_{marine}) is rather low and increases with increasing distance to the glacier termini. The f_{marine} value was estimated using an isotope mass balance based on F^{14}C of the bulk TOC, with two endmembers: one modern OC_{marine} (F^{14}C ≈ 1 = modern) and one fossil OC_{petro} (F^{14}C = 0 = fossil; Methods). The short core in the vicinity of glacier termini and the long core in the centre of the Brepollen basin both have low f_{marine} values of 2 ± 2 to 11 ± 2%. By contrast, in the short core (He519_2-3) from the fjord main basin, the f_{marine} ranges from 42 ± 2% at the core top to 26 ± 6% at the bottom. Overall, the TOC age is primarily controlled by the input of OC_{marine} as this input is the main difference between the OC deposited in the main basin versus the Brepollen basin.

Compound-specific radiocarbon analysis

Owing to the characteristic F^{14}C signature of the two pools, we were able to use ^{14}C as an inverse tracer (absence of ^{14}C) under the assumption that the isotopic signature of the substrate (that is, in sediments) will be passed on through the heterotrophic utilization into the synthesized biomass[3]. Following the approach of ref. 3, we assessed the bioavailability of these two OC pools in the sediment cores by radiocarbon analyses of the fatty acid (FA) side chains of intact polar lipids (IPLs; IPL–FAs), extracted with a modified ref. 38 approach. Bacterial IPLs have been reported to decay within days to weeks after cell lysis and are therefore regarded as indicators for living microbiota[39]. Bacterially produced FAs $C_{br-15:0}$ and $C_{16:1n-7}$[5] were purified into single-compound fractions and subsequently radiocarbon dated. With this approach, we were able to identify the average F^{14}C signature of the substrate utilized by bacteria in the sediment[5]. To ensure bacterial FA origin, precursor lipids were determined by high-pressure liquid chromatography coupled to mass spectrometry (HPLC–MS).

Using HPLC–MS, the dated $C_{br-15:0}$ and $C_{16:1n-7}$ FAs were found to derive from a diverse group of phospholipid precursors: mainly phosphatidylglycerol and phosphatidylethanolamine in the glacier termini and Brepollen long core, and additionally phosphatidylcholine in the main basin core (Supplementary Fig. 1). While most of these lipids can be assigned to sulfate-reducing bacteria[40] or other sedimentary marine bacteria[41], minor contributions of potentially algae-derived betaine lipids and phosphatidylcholine (<10%) could potentially lead to an increase in the measured F^{14}C FA values and hence an underestimation of OC_{petro} degradation (Supplementary Information).

In the marine-influenced main basin core (He519_2-3), compound-specific F^{14}C values for IPL–FAs within the topmost part of the core (<15 cm; F^{14}C = 0.939 ± 0.008 to 1.002 ± 0.009) agree closely with modelled surface dissolved inorganic carbon (DIC) values (F^{14}C = 1.013 ± 0.015 to 1.116 ± 0.020), indicating an exclusive or at least strong preferential utilization of recently synthesized OC_{marine} (Fig. 3a). Further downcore (17–21 and 21–24 cm), the FAs diverge from modelled DIC signatures towards lower F^{14}C values (F^{14}C < 1.000 ± 0.007), indicating an increase in OC_{petro} utilization. Interestingly, this shift mirrors a decrease of f_{marine} from 30 to 42% in the topmost 15 cm to less than 30% below. Nevertheless, OC_{marine} is the primary, but not exclusive, substrate utilized by the sedimentary microbiome in sediment core He519_2-3, while an apparent shift towards increasing OC_{petro} utilization occurs downcore.

A different picture emerges at the glacier termini core (He560_26-2-K1; Fig. 3e). The $C_{16:1n-7}$ F^{14}C values range between 0.767 ± 0.011 and 0.697 ± 0.016, which is far lower and outside the 2σ uncertainty of the modelled surface DIC F^{14}C (ranging between 1.009 ± 0.015 and 1.023 ± 0.015). This indicates the substantial uptake of OC_{petro} into the bacterial membrane lipids. Unfortunately, sedimentary contents of $C_{br-15:0}$ were too low to perform compound-specific radiocarbon dating. IPL–FA data from the Brepollen long core (HH14-897-GC-MF; Fig. 3c) show F^{14}C values similar to those from the He560 glacier termini core
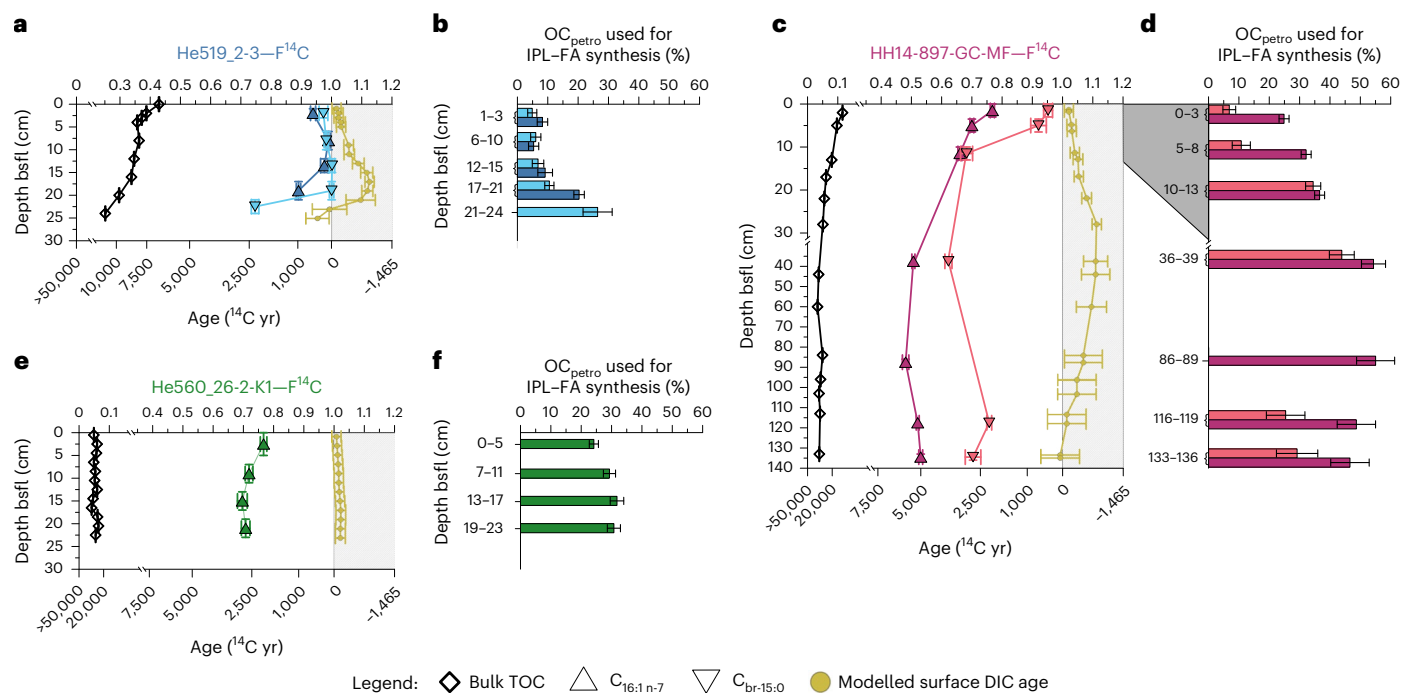
Fig. 3 | IPL–FA radiocarbon data and estimated OC$_{petro}$ used for IPL–FA synthesis. a–f, Colour-coded data from sediment cores He519_2-3 (blue; **a,b**), HH14-897-GC-MF (purple; **c,d**) and He560_26-2-K1 (green; **e,f**). Panels **a**, **c** and **e** display radiocarbon signatures of TOC, modelled surface DIC and IPL–FAs (C$_{16:1 n-7}$ and C$_{br-15:0}$) displayed as fraction of modern carbon (F^{14}C) values and corresponding ^{14}C age. Values in the grey-shaded area show elevated F^{14}C values (>1), due to 1960s above-ground nuclear weapons tests, thus giving the impression of apparent ages in ^{14}C years in the future. Data are presented as mean values for blank corrected measured (TOC, IPL–FA) and calculated values (surface DIC F^{14}C signature and panels **b,d,f**). Panels **b**, **d** and **f** represent calculated percentages of OC$_{petro}$ used for bacterial IPL–FA synthesis of C$_{16:1 n-7}$ (dark coloured) and C$_{br-15:0}$ (light coloured). Values are estimated by an isotope mass balance using respective IPL–FA F^{14}C signatures (**a,c,e**) versus the endmembers of fossil OC$_{petro}$ (F^{14}C = 0) and modelled surface DIC F^{14}C signature in the calendar year of deposition (Methods). Please note the different axis breaks in **c** and **d**. Vertical error bars in **a**, **c** and **e** display depth intervals of analysed sediments. Uncertainties in **a**, **c** and e for bulk TOC, IPL–FA C$_{16:1 n-7}$ and C$_{br-15:0}$ display propagated 1σ errors of measurements and blank correction (Methods); uncertainties displayed in the modelled surface DIC F^{14}C signatures are propagated 1σ errors from the sediment age model combined with an estimated F^{14}C (DIC) uncertainty of 0.015. Uncertainties displayed in **b**, **d** and **f** represent propagated 1σ uncertainties from **a**, **c** and **e** of measured IPL–FAs (C$_{16:1 n-7}$ and C$_{br-15:0}$) and modelled surface DIC age uncertainties.

at the topmost interval. As depth increases, the IPL–FA signatures shift towards even lower F^{14}C values, reflecting increasing OC$_{petro}$ utilization in sediments, representing depositions closer to the glacier termini. The values remain rather constant below 30 cm. This shift occurs alongside a decrease in the f_{marine} in the sediments—similar to the decrease in the main basin core. The pervasive offset in F^{14}C values between C$_{16:1 n-7}$ and C$_{br-15:0}$ can best be explained by different bacterial sources for these IPL–FAs that preferentially consume different types of organic matter (Supplementary Information).

The percentage of ancient carbon used for the microbial biosynthesis (Fig. 3b,d,f) was estimated with an isotope mass balance model, using a radiocarbon-free fossil endmember for OC$_{petro}$ (F^{14}C = 0) and modern OC$_{marine}$ endmember according to the reservoir age modelled at the respective depth intervals (Methods). A pronounced difference between the two Brepollen cores and the main basin core is evident from this mass balance estimate. Within the top 15 cm of the main basin core, OC$_{petro}$ accounts for 5 ± 2 to 9 ± 2% of the utilized carbon, whereas in the Brepollen cores, OC$_{petro}$ contributes up to 37 ± 2% in the topmost intervals. The most proximal core at the glacier termini is characterized by extremely high sedimentation rates, f_{marine} values consistently below 6 ± 2% throughout the core and fairly constant OC$_{petro}$ utilization (24 ± 2 to 32 ± 2%). On the contrary, in both the marine-influenced main basin short core and the central Brepollen basin long core, we can observe an increased utilization of OC$_{petro}$ with increasing depth and decreasing f_{marine}. The highest estimate of OC$_{petro}$ utilization reached 55 ± 6% in the central Brepollen core in the depth interval of 86–89 cm, compared with the lowest OC$_{petro}$ of only 5 ± 6% in the marine-influenced main

basin core (see above). Here, we show that even over short distances within one fjord system the microbial utilization of OC$_{petro}$ can vary widely, suggesting both low and substantial fossil GHG emission potential from increasing glacial erosion.

Although we cannot directly identify the mechanisms for OC$_{petro}$ utilization, we hypothesize that with decreasing abundance of fresh, labile OC$_{marine}$, micro-organisms are forced to utilize OC$_{petro}$ for their biosynthesis. For example, in the interval with the highest percentage of OC$_{petro}$ utilized for lipid synthesis (HH14, 86–89 cm) the mass balance suggests that 55 ± 6% of utilized carbon originates from OC$_{petro}$ when the abundance of labile OC$_{marine}$ in the sediment is low (f_{marine} = 5 ± 6%). In the topmost three dated intervals of the main basin core, OC$_{petro}$ utilization is much lower, but still accounts for 5 ± 2 to 9 ± 2% when f_{marine} is above 30%.

Under the assumption that sedimentary micro-organisms use the same substrate for both their anabolic and catabolic pathways[42], we estimate that heterotrophic remineralization of OC$_{petro}$ accounts for between 5 ± 2 and 55 ± 6% of local microbiota's overall energy consumption. This remineralization leads to the conclusion that CO$_2$ (and CH$_4$) emitted from sediments as metabolic end-products originates in some part from fossil sources, which might be enhanced with increased mobilization of ancient organic-rich deposits in a warming climate.

Implications of OC$_{petro}$ utilization

Our data indicate that OC$_{petro}$ is indeed microbially utilized after deposition in Hornsund Fjord. These findings are in line with previous studies[3,6,11,12] and highlight that several parts of the world's OC$_{petro}$ pools are

part of the active carbon cycle, and that these may be affected by microbial processing and consumption. Glaciated fjord ecosystems similar to the Hornsund Fjord with often OC-rich (including coal-bearing) bedrock in their drainage areas are fairly widespread and can be found in Svalbard[43], Alaska[44], Greenland[45], Franz Josef Land[46] and Antarctica[47]. These ecosystems may likewise supply suitable substrates for microbial degradation to marine sediments. Recent studies of other glacial environments based on modern glacial sediments[48], watershed analysis[12] and palaeo CO_2 isotopic compositions[10] indicate that similar utilization of old, previously 'locked up' OC may also occur onshore, indicating the geographical pervasiveness of OC_{petro} utilization. Microbial OC_{petro} utilization has also been reported from terrestrial shales[3]. These findings indicate that OC_{petro} utilization at the rock interface, after erosion and redeposition, is likely to occur globally. The resulting fossil GHG emissions may be substantial on a geological timescale—even if only a fraction of the OC_{petro} becomes remineralized after deposition or exposure.

Based on our data, we cannot estimate GHG fluxes resulting from OC_{petro} utilization in marine sediments. However, considering the size of the global OC_{petro} reservoir[1], further quantitative research into this topic seems to be mandated, both in terms of a global OC_{petro} flux from rivers, ice sheets and glaciers, and OC_{petro} utilization dynamics in sediments, soils and the water column. High-latitude temperatures continue to rise up to four times more rapidly than in the rest of the world[49], and sediment export rates are expected to increase from both glaciers[21] and ice sheets[22] to downstream depositional environments. Next to oxidation of OC_{petro}, increases in fertilization of primary production[25] and turbidity[24] are just two of the consequent manifold associated environmental changes impacting carbon cycling in the glacial environment. Considering a recent estimate of global atmospheric CO_2 concentrations increasing by 50 ppm due to fjord sediment mobilization during the Last Glacial Maximum[50], a potential climate impact on decadal to centennial timescales seems worth investigating. Therefore, to fully grasp the impact of glacial retreat on global carbon budgets, studying these processes in both marine and terrestrial settings may be needed, given the Intergovernmental Panel on Climate Change projections based on the low-emission Representative Concentration Pathway 2.6 scenario, which predict global glacial mass loss of 18% in 2100 relative to 2015, suggesting long-lasting effects even in the event of zero anthropogenic GHG emissions[20].

Online content

Any methods, additional references, Nature Portfolio reporting summaries, source data, extended data, supplementary information, acknowledgements, peer review information; details of author contributions and competing interests; and statements of data and code availability are available at https://doi.org/10.1038/s41561-023-01198-z.

References

1. Galy, V. et al. Recycling of graphite during Himalayan erosion: a geological stabilization of carbon in the crust. *Science* **322**, 943–945 (2008).
2. Guillemette, F. et al. Old before your time: ancient carbon incorporation in contemporary aquatic foodwebs. *Limnol. Oceanogr.* **62**, 1682–1700 (2017).
3. Petsch, S. T. et al. ^{14}C-dead living biomass: evidence for microbial assimilation of ancient organic carbon during shale weathering. *Science* **292**, 1127–1131 (2001).
4. Cui, X. et al. Erosion of modern terrestrial organic matter as a major component of sediments in fjords. *Geophys. Res. Lett.* **44**, 1457–1465 (2017).
5. Wakeham, S. G. et al. Natural-abundance radiocarbon as a tracer of assimilation of petroleum carbon by bacteria in salt marsh sediments. *Geochim. Cosmochim. Acta* **70**, 1761–1771 (2006).
6. Hemingway, J. D. et al. Microbial oxidation of lithospheric organic carbon in rapidly eroding tropical mountain soils. *Science* **360**, 209–212 (2018).
7. Petsch, S. T. (2013). Weathering of Organic Carbon. In Treatise on Geochemistry: Second Edition (Vol. 12, pp. 217–238). Elsevier Inc. https://doi.org/10.1016/B978-0-08-095975-7.01013-5
8. France-Lanord, C. & Derry, L. A. Organic carbon burial forcing of the carbon cycle from Himalayan erosion. *Nature* **390**, 65–67 (1997).
9. Berner, R. A. & Caldeira, K. The need for mass balance and feedback in the geochemical carbon cycle. *Geology* **25**, 955–956 (1997).
10. Blattmann, T. M. Ideas and perspectives: emerging contours of a dynamic exogenous kerogen cycle. *Biogeosciences* **19**, 359–373 (2022).
11. Soulet, G. et al. Temperature control on CO_2 emissions from the weathering of sedimentary rocks. *Nat. Geosci.* **14**, 665–671 (2021).
12. Horan, K. et al. Mountain glaciation drives rapid oxidation of rock-bound organic carbon. *Sci. Adv.* **3**, e1701107 (2017).
13. Hilton, R. G. et al. Geological respiration of a mountain belt revealed by the trace element rhenium. *Earth Planet. Sci. Lett.* **403**, 27–36 (2014).
14. Hood, E. et al. Glaciers as a source of ancient and labile organic matter to the marine environment. *Nature* **462**, 1044–1047 (2009).
15. Hemingway, J. D. et al. Mineral protection regulates long-term global preservation of natural organic carbon. *Nature* **570**, 228–231 (2019).
16. Kohler, T. J. et al. Patterns in microbial assemblages exported from the meltwater of Arctic and sub-Arctic glaciers. *Front. Microbiol.* **11**, 669 (2020).
17. Smith, R. W. et al. High rates of organic carbon burial in fjord sediments globally. *Nat. Geosci.* **8**, 450–453 (2015).
18. Hood, E. et al. Storage and release of organic carbon from glaciers and ice sheets. *Nat. Geosci.* **8**, 91–96 (2015).
19. Bennett, M. M. & Glasser, N. F. *Glacial Geology: Ice Sheets and Landforms* (John Wiley & Sons, 2011).
20. IPCC *Special Report on the Ocean and Cryosphere in a Changing Climate* (2019).
21. Delaney, I. & Adhikari, S. Increased subglacial sediment discharge in a warming climate: consideration of ice dynamics, glacial erosion, and fluvial sediment transport. *Geophys. Res. Lett.* **47**, (2020).
22. Bendixen, M. et al. Delta progradation in Greenland driven by increasing glacial mass loss. *Nature* **550**, 101–104 (2017).
23. Szczuciński, W. et al. Sediment accumulation rates in subpolar fjords – impact of post-Little Ice Age glaciers retreat, Billefjorden, Svalbard. *Estuar. Coast. Shelf Sci.* **85**, 345–356 (2009).
24. Szczuciński, W. & Zajączkowski, M. in *Sediments, Morphology and Sedimentary Processes on Continental Shelves: Advances in Technologies, Research, and Applications* (eds Li, M. Z. et al.) 369–386 (International Association of Sedimentologists, 2012).
25. Bhatia, M. P. et al. Organic carbon export from the Greenland ice sheet. *Geochim. Cosmochim. Acta* **109**, 329–344 (2013).
26. Drenzek, N. J. et al. Constraints on the origin of sedimentary organic carbon in the Beaufort Sea from coupled molecular ^{13}C and ^{14}C measurements. *Mar. Chem.* **103**, 146–162 (2007).
27. Błaszczyk, M. et al. Fluctuations of tidewater glaciers in Hornsund Fjord (southern Svalbard) since the beginning of the 20th century. *Pol. Polar Res.* **34**, 327–352 (2013).
28. Birkenmajer, K. Geology of the Hornsund area, Spitsbergen. *Katowice, Pol.* **1**, 1–42 (1990).
29. Włodarska-Kowalczuk, M. et al. Organic carbon origin, benthic faunal consumption, and burial in sediments of northern Atlantic and Arctic fjords (60–81° N). *J. Geophys. Res. Biogeosci.* **124**, 3737–3751 (2019).

30. Ćmiel, S. R. & Fabiańska, M. J. Geochemical and petrographic properties of some Spitsbergen coals and dispersed organic matter. *Int. J. Coal Geol.* **57**, 77–97 (2004).

31. Harland, W. B. *The Geology of Svalbard* Ch. 20, Geological Society Memoir No. 17 (The Geological Society, 1997).

32. Szczuciński, W. et al. Climate-driven variations in source-to-sink fluxes of sediment and carbon in High Arctic fjord (Hornsund, Svalbard). In *33rd International Meeting of Sedimentology and 16ème Congrés Français Sédimentologie, Toulouse* 10–12 (2017).

33. Meyers, P. A. Organic geochemical proxies of paleoceanographic, paleolimnologic, and paleoclimatic processes. *Org. Geochem.* **27**, 213–250 (1997).

34. Hopmans, E. C. et al. A novel proxy for terrestrial organic matter in sediments based on branched and isoprenoid tetraether lipids. *Earth Planet. Sci. Lett.* **224**, 107–116 (2004).

35. Bray, E. E. & Evans, E. D. Distribution of *n*-paraffins as a clue to recognition of source beds. *Geochim. Cosmochim. Acta* **22**, 2–15 (1961).

36. Piwosz, K. et al. Comparison of productivity and phytoplankton in a warm (Kongsfjorden) and a cold (Hornsund) Spitsbergen fjord in mid-summer 2002. *Polar Biol.* **32**, 549–559 (2009).

37. Meire, L. et al. Marine-terminating glaciers sustain high productivity in Greenland fjords. *Glob. Change Biol.* **23**, 5344–5357 (2017).

38. Slater, G. F. et al. Intrinsic bacterial biodegradation of petroleum contamination demonstrated in situ using natural abundance, molecular-level ^{14}C analysis. *Org. Geochem.* **37**, 981–989 (2006).

39. Logemann, J. et al. A laboratory experiment of intact polar lipid degradation in sandy sediments. *Biogeosciences* **8**, 2547–2560 (2011).

40. Seidel, M. et al. Phosphate-free ornithine lipid contents in *Desulfovibrio* spp. respond to growth temperature. *Org. Geochem.* **59**, 133–142 (2013).

41. Schubotz, F. et al. Petroleum degradation and associated microbial signatures at the Chapopote asphalt volcano, southern Gulf of Mexico. *Geochim. Cosmochim. Acta* **75**, 4377–4398 (2011).

42. Carlson, C. A. et al. Microbes and the dissipation of energy and respiration: from cells to ecosystems. *Oceanography* **20**, 89–100 (2007).

43. Kim, J.-H. et al. Large ancient organic matter contributions to Arctic marine sediments (Svalbard). *Limnol. Oceanogr.* **56**, 1463–1474 (2011).

44. Page, D. S. et al. The natural petroleum hydrocarbon background in subtidal sediments of Prince William Sound, Alaska, USA. *Environ. Toxicol. Chem. Int. J.* **15**, 1266–1281 (1996).

45. Bojesen-Koefoed, J. A. et al. A remote coal deposit revisited: Middle Jurassic coals at Kulhøj, western Germania Land, northeast Greenland. *Int. J. Coal Geol.* **98**, 50–61 (2012).

46. Dibner, V. D. et al. The geology of Franz Josef Land archipelago, Russian Federation (1992).

47. Elliot, D. H. et al. Age provinces in the Antarctic craton: evidence from detrital zircons in Permian strata from the Beardmore Glacier region, Antarctica. *Gondwana Res.* **28**, 152–164 (2015).

48. Vinšová, P. et al. The biogeochemical legacy of Arctic subglacial sediments exposed by glacier retreat. *Glob. Biogeochem. Cycles* **36**, (2022).

49. Rantanen, M. et al. The Arctic has warmed nearly four times faster than the globe since 1979. *Commun. Earth Environ.* **3**, 168 (2022).

50. Cui, X. et al. Global fjords as transitory reservoirs of labile organic carbon modulated by organo–mineral interactions. *Sci. Adv.* **8**, 0610 (2022).

Methods

Sampling

The sediment cores analysed in this study were taken on three separate expeditions in Hornsund Fjord, Svalbard. Gravity core HH14-897-MF-GC was taken in October 2014 onboard the Norwegian RV *Helmer Hanssen* in the central Brepollen basin. The two short cores were taken on the German RV *Heincke* during cruises He519 in September 2018 and He560 in August 2020. Core He519_2-3 was taken at the central main basin, whereas core He560_26-2-K1 was retrieved in the inner Brepollen basin (Supplementary Table 2).

Both short cores were sliced onboard RV *Heincke*, transferred into glass containers and frozen at −20 °C immediately after coring until analysis. The archive half of gravity core HH14-897-MF-GC was stored at 4 °C in the core repository at the Department of Geosciences, UiT The Arctic University of Norway, prior to sampling in January 2019. After sampling, sediments were transferred into glass containers and stored at −20 °C. Even though the long sediment core was not frozen immediately after coring, biomarkers, bulk parameters, compound-specific radiocarbon data and IPL data show similar patterns to the second Brepollen basin core He560_26-2-K1. In particular, the matching IPL (Supplementary Information) and compound-specific radiocarbon data provide confidence that the data obtained from the Brepollen long core accurately reflect in-situ information and allow for OC_{petro} utilization estimates in the deeper core sections. Any potential storage effects would be expected to result in increased IPL concentrations and $F^{14}C$ values of IPL biased towards modern atmospheric values, which was not observed.

All glassware used was combusted at 450 °C for 6 hours and equipment cleaned with solvents before usage for both sampling and laboratory activities.

Age models

The age models were established using the short-lived isotopes ^{210}Pb and ^{137}Cs. The ^{210}Pb in recent marine sediments is of twofold origin. The supported ^{210}Pb ($^{210}Pb_{sup}$) is continuously produced within the sediments by the decay of parent isotopes, while excess ^{210}Pb ($^{210}Pb_{ex}$) is delivered to the sediment from above, produced by ^{222}Rn decay in the atmosphere and the water column overlying the sediment. Sediment cores He519_2-3 and He560_26-2-K1 were analysed at the Alfred Wegener Institute Bremerhaven, Germany, using a planar-type high-purity germanium (HPGe) gamma spectrometer. Core HH14-897-GC-MF was measured at the Institute of Geology at Adam Mickiewicz University in Poznań, Poland, using a gamma detector Canberra BE3830. The age models of the three cores were generated based on $^{210}Pb_{ex}$ using the constant flux–constant sedimentation (CFCS) model and verified with penetration depth and peaks in ^{137}Cs isotope and historical information on the fjord deglaciation[27]. However, alternative models were also considered and the resulting accumulation rates should be regarded as approximates as the particular assumptions behind each model were not fully met. The analysis was conducted with the help of the R-based serac code[51] (Supplementary Figs. 4–6).

Surface DIC age model

Dissolved inorganic radiocarbon concentrations of surface water are simulated using the Finite-volumE Sea ice–Ocean Model (FESOM2)[52] equipped with radiocarbon[53]. Radiocarbon is implemented in terms of $F^{14}C$, neglecting marine biological processes, which play a minor role compared with circulation and radioactive decay[54,55]. Air–sea exchange fluxes of $^{14}CO_2$ in FESOM2 depend on wind speed and CO_2 solubility[56], and assume a surface water global mean DIC concentration of 2.0 mol m^{-3}. The model was spun up in a previous simulation to quasi steady-state conditions typical of 1850[53]. We continued the simulation to 2015, using periodic climate forcing[57] and transient values of atmospheric CO_2 (ref. 58) and of $F^{14}C$ (ref. 59). In the North Atlantic, the simulated anthropogenic ^{14}C distribution is in line with

observations[60,61]. FESOM2 employs unstructured meshes with variable resolution, here featuring about 127,000 surface nodes and 47 layers. After the simulation, the model results were remapped to regular geographical coordinates and evaluated at the surface level considering the grid cell nearest to Hornsund.

TOC and stable carbon isotope ratios

TOC concentrations of core HH14-897-MF-GC were measured at the Department of Quaternary Geology and Palaeogeography of the Adam Mickiewicz University. The analyses were performed with a vario MAX CNS elemental analyser (Elementar). To determine the OC content, prior to the analyses, samples were treated with 1 M liquid hydrochloric acid (HCl) at room temperature for over a week (until no sign of reaction is visible) to remove carbonates. The $\delta^{13}C$ of bulk OC in sediment was obtained using a Flash EA 1112 HT elemental analyser combined with a Thermo DELTA V Advantage isotopic ratio mass spectrometer in a continuous-flow mode. Results are expressed relative to Vienna PeeDee Belemnite. Methods are described in detail in ref. 62. The preliminary results were presented by ref. 32.

Both sediment cores He519_2-3 and He560_26-2-K1 were analysed for TOC and $\delta^{13}C$ by continuous-flow elemental analyser–isotope ratio mass spectrometer using a Thermo Finnigan Flash EA 2000 connected to a Delta V Plus isotope ratio mass spectrometer at MARUM, Bremen, Germany, following the protocols of ref. 63 and ref. 64. Pre-treatment involved sample homogenization and carbonate removal overnight with 10% HCl or until no further gas development was visible. Afterwards the sample was neutralized with deionized water, freeze-dried and weighed for analysis.

Bulk radiocarbon dating

Radiocarbon ages of the TOC were determined by accelerator mass spectrometry at the MICADAS facility of the Alfred Wegener Institute. Accelerator mass spectrometry dating was performed on graphite targets of 1 mgC, and sediment masses were chosen according to TOC concentrations. As a pre-treatment, samples were homogenized and carbonates were removed three times with 6 M HCl at 60 °C. Methodology and blank determination were performed as described in ref. 65.

Lipid biomarkers

Lipid biomarkers were extracted from about 3 g of sediment using the method by ref. 66 at the Alfred Wegener Institute and subsequently separated into four subfractions for alkanes, ketones, alcohols (containing glycerol dialkyl glycerol tetraethers: GDGTs) and FAs, as described in ref. 67. The subfractions of alkanes and FAs were quantified on a GC–FID on a setup as in ref. 67. GDGTs were quantified on a HPLC–MS setup as described in ref. 67, after the protocol of ref. 68. Known amounts of the internal standards squalane, C_{46}-GDGT and 19-methylarachidic acid were added to the sediments before the extraction for the quantification of alkanes, GDGTs and FAs, respectively.

Subsequently, biomarker indices were calculated as follows:

- CPI indicating thermal maturity of OC, using the ratio of even to odd numbered *n*-alkanes after ref. 35:

$$CPI = 0.5 \times \left(\frac{C_{25} + C_{27} + C_{29} + C_{31} + C_{33}}{C_{24} + C_{26} + C_{28} + C_{30} + C_{32}} + \frac{C_{25} + C_{27} + C_{29} + C_{31} + C_{33}}{C_{26} + C_{28} + C_{30} + C_{32} + C_{34}} \right) \quad (1)$$

- BIT index indicating input from terrestrial soils in the catchment area (and absence thereof in the case of values near 0) after ref. 34:

$$BIT\ index = \frac{GDGT\ I + GDGT\ II + GDGT\ III}{Crenarchaeol + GDGT\ I + GDGT\ II + GDGT\ II} \quad (2)$$

- TAR indicating the relative abundance of OC from terrestrial versus aquatic origin, using comparison of short- and long-chain FA concentrations, after ref. 33:

$$TAR = \frac{C_{24:0} + C_{26:0} + C_{28:0}}{C_{12:0} + C_{14:0} + C_{16:0}} \qquad (3)$$

IPLs

IPLs were extracted with a ref. [69] approach, following the protocol by ref. [38]; depth intervals of the individual cores were chosen to obtain at least 80 g of sediment to ensure sufficient FA recovery for subsequent radiocarbon analysis. The total lipid extracts were separated into three fractions via an activated (1% H_2O) silica column chromatography into neutral lipids, glyco lipids and polar lipids using dichloromethane, acetone and methanol, respectively, to elute the fractions from the column, following the methodologies of ref. [38], ref. [5] and ref. [70], respectively.

Aliquots of 1% of the polar lipid fractions were analysed on a Bruker maXis Plus ultra-high-resolution quadrupole time-of-flight mass spectrometer with an electrospray ionization source coupled to Dionex Ultimate 3000RS ultra-high-pressure liquid chromatography at MARUM, Bremen. The analyses were carried out using hydrophilic interaction chromatography in positive mode to check the separation of phospholipids with improved chromatographic separation and detection as described in ref. [71].

Compound-specific radiocarbon analysis

Compound-specific radiocarbon analysis (CSRA) was performed on purified IPL–FA and n-alkanes from aliquots obtained by modified Bligh and Dyer extraction[69] as described above. IPL–FA CSRA was performed of all extracted depth intervals. CSRA of n-alkanes purified from the neutral fraction was limited to three depth intervals (0–3, 86–89 and 133–136 cm) of core HH14-897-MF-GC. The n-alkane separation for CSRA was achieved following methods described by Meyer et al.[72].

The polar lipid fractions were saponified at 80 °C with 1 ml of KOH (0.1 M) in MeOH:H_2O (9:1, v/v) for 2 h. Neutral lipids were removed with a liquid–liquid phase separation using hexane. The remaining solution was acidified and FAs were extracted with a liquid–liquid phase separation using dichlormethan. The FAs were converted into fatty acid methyl esters (FAMEs) overnight at 50 °C in MeOH at a pH of 1 under a N_2 atmosphere. Subsequently, the FAMEs were separated from the MeOH phase by liquid–liquid phase separation using hexane and purified via passage through an activated (1% H_2O) silica column, eluting FAMEs with 4 ml dichlormethan:hexan (2:1, v/v).

From both of the purified n-alkane and IPL–FA methyl ester fractions, single compounds were isolated using a gas chromatograph coupled to a preparative fraction collector (PFC) with the setup described in ref. [73]. CSRA was performed as gas measurements at the MICADAS facility of the Alfred Wegener Institute following the protocol described in ref. [65].

Blank determination for CSRA was achieved in a two-step process. (1) Procedural blanks were run alongside the samples to ensure that no contamination from glassware, solvents or reagents occurred during the extraction and wet chemical preparation. All blanks were free of those FA and n-alkane homologues that were subsequently isolated with PFC. (2) Procedural blanks for PFC and subsequent radiocarbon analysis were determined using FAs and n-alkanes extracted from recent (apple peel) and fossil (Eocene Messel shale) laboratory internal standard materials, followed by subsequent radiocarbon age correction with according blanks as described in ref. [74] and ref. [75].

Isotope mass balance

The isotope mass balance calculations used a fossil, $F^{14}C_{fossil}$, and a modern endmember, $F^{14}C_{modelled\ DIC}$. The fossil endmember was set to a constant $F^{14}C$ value of 0, as the OC_{petro} is expected to be radiocarbon-free, as organic-rich rocks outcropping the hinterland of Hornsund were deposited in the Tertiary[76,77]. Further, compound-specific radiocarbon analyses of isolated n-alkanes yielded $F^{14}C$ values near the detection limit, supporting the radiocarbon-free endmember definition (Supplementary Information). The modern endmember was defined as equivalent to the modelled surface DIC radiocarbon signature based on the biomarker data. The biomarker data indicated that the organic matter originated exclusively from the fixation of DIC during photosynthesis and OC from primary production is assumed to have the same radiocarbon signature. $F^{14}C_{modelled\ DIC}$ values changed over time due to the rapid decrease in the $F^{14}C$ of the modelled surface DIC after the peak in atmospheric radiocarbon content resulting from above-ground nuclear weapons tests in the 1960s (Supplementary Fig. 7). Therefore, for the calculations, the $F^{14}C_{modelled\ DIC}$ was adjusted according to the estimated year of sediment deposition, based on $^{210}Pb + ^{137}Cs$ age models as described above.

The isotopic mass balances were used to estimate the relative contribution of OC_{marine} (f_{marine}) to the bulk sedimentary OC and to calculate the percentage of OC_{marine} used for bacterial membrane lipid synthesis (%$OC_{marine-synt}$) based on the $F^{14}C$ signatures of the bulk TOC ($F^{14}C_{bulk}$) and the dated single-compound IPL–FAs ($F^{14}C_{IPL-FA}$). The general equations used for the calculations are:

$$F^{14}C_{fossil} \qquad (4)$$

$$F^{14}C_{modelled\ DIC} \qquad (5)$$

Data availability

All obtained data are publicly available at the PANGEA data repository (https://doi.org/10.1594/PANGAEA.946019). Bulk data of core HH14-897-GC-MF, including bulk TOC and $\delta^{13}C$, ^{210}Pb and ^{137}Cs measurements (https://doi.org/10.1594/PANGAEA.946568), as well as the associated age model (https://doi.org/10.1594/PANGAEA.946576), are available separately on PANGEA.

References

51. Bruel, R. & Sabatier, P. serac: an R package for ShortlivEd RAdionuclide Chronology of recent sediment cores. *J. Environ. Radioact.* **225**, 106449 (2020).
52. Danilov, S. et al. The Finite-volumE Sea ice–Ocean Model (FESOM2). *Geosci. Model Dev.* **10**, 765–789 (2017).
53. Lohmann, G. et al. Abrupt climate and weather changes across time scales. *Paleoceanogr. Paleoclimatol.* **35**, (2020).
54. Fiadeiro, M. E. Three-dimensional modeling of tracers in the deep Pacific Ocean II. Radiocarbon and the circulation. *J. Mar. Res.* **40**, 537–550 (1982).
55. Toggweiler, J. R. et al. Simulations of radiocarbon in a coarse-resolution world ocean model: 1. Steady state prebomb distributions. *J. Geophys. Res. Ocean.* **94**, 8217–8242 (1989).
56. Wanninkhof, R. Relationship between wind speed and gas exchange over the ocean revisited. *Limnol. Oceanogr. Methods* **12**, 351–362 (2014).
57. Large, W. G. & Yeager, S. G. The global climatology of an interannually varying air–sea flux data set. *Clim. Dyn.* **33**, 341–364 (2009).
58. Meinshausen, M. et al. Historical greenhouse gas concentrations for climate modelling (CMIP6). *Geosci. Model Dev.* **10**, 2057–2116 (2017).
59. Graven, H. et al. Compiled records of carbon isotopes in atmospheric CO_2 for historical simulations in CMIP6. *Geosci. Model Dev.* **10**, 4405–4417 (2017).
60. Key, R. M. et al. A global ocean carbon climatology: results from Global Data Analysis Project (GLODAP). *Glob. Biogeochem. Cycles* **18**, GB4031 (2004).
61. Butzin, M., Sidorenko, D. & Köhler, P. A multi-resolution ocean simulation of the anthropogenic radiocarbon transient. In *EGU General Assembly 2021* https://doi.org/10.5194/EGUSPHERE-EGU21-3118 (2021).

62. Woszczyk, M. et al. Effects of environmental history and post-depositional processes on the organic matter record of Lake Łebsko, Poland. *Org. Geochem.* **155**, 104209 (2021).

63. Werner, R. A. & Brand, W. A. Referencing strategies and techniques in stable isotope ratio analysis. *Rapid Commun. Mass Spectrom.* **15**, 501–519 (2001).

64. Brodie, C. R. et al. Evidence for bias in C and N concentrations and $\delta^{13}C$ composition of terrestrial and aquatic organic materials due to pre-analysis acid preparation methods. *Chem. Geol.* **282**, 67–83 (2011).

65. Mollenhauer, G. et al. Standard operation procedures and performance of the MICADAS radiocarbon laboratory at Alfred Wegener Institute (AWI), Germany. *Nucl. Instrum. Methods Phys. Res. B* **496**, 45–51 (2021).

66. Mollenhauer, G. & Eglinton, T. I. Diagenetic and sedimentological controls on the composition of organic matter preserved in California Borderland basin sediments. *Limnol. Oceanogr.* **52**, 558–576 (2007).

67. Wei, B. et al. Comparison of the $U_{37}^{K'}$, LDI, TEX_{86}^{H}, and RI–OH temperature proxies in sediments from the northern shelf of the South China Sea. *Biogeosciences* **17**, 4489–4508 (2020).

68. Hopmans, E. C. et al. The effect of improved chromatography on GDGT-based palaeoproxies. *Org. Geochem.* **93**, 1–6 (2016).

69. Bligh, E. G. & Dyer, W. J. A rapid method of total lipid extraction and purification. *Can. J. Biochem. Physiol.* **37**, 911–917 (1959).

70. Akondi, R. N. et al. Modified lipid extraction methods for deep subsurface shale. *Front. Microbiol.* **8**, 1408 (2017).

71. Wörmer, L. et al. Application of two new LC–ESI–MS methods for improved detection of intact polar lipids (IPLs) in environmental samples. *Org. Geochem.* **59**, 10–21 (2013).

72. Meyer, V. D. et al. Permafrost-carbon mobilization in Beringia caused by deglacial meltwater runoff, sea-level rise and warming. *Environ. Res. Lett.* **14**, 085003 (2019).

73. Wei, B. et al. The nature, timescale, and efficiency of riverine export of terrestrial organic carbon in the (sub)tropics: insights at the molecular level from the Pearl River and adjacent coastal sea. *Earth Planet. Sci. Lett.* **565**, 116934 (2021).

74. Winterfeld, M. et al. Deglacial mobilization of pre-aged terrestrial carbon from degrading permafrost. *Nat. Commun.* **9**, 3666 (2018).

75. Sun, S. et al. ^{14}C blank assessment in small-scale compound-specific radiocarbon analysis of lipid biomarkers and lignin phenols. *Radiocarbon* **62**, 207–218 (2020).

76. Lewińska-Preis, L. et al. Geochemical distribution of trace elements in Kaffioyra and Longyearbyen coals, Spitsbergen, Norway. *Int. J. Coal Geol.* **80**, 211–223 (2009).

77. Marshall, C. et al. Geochemistry and petrology of palaeocene coals from Spitzbergen — Part 2: Maturity variations and implications for local and regional burial models. *Int. J. Coal Geol.* **143**, 1–10 (2015).

Author contributions

All authors contributed extensively to the work presented in this paper. M.R., G.M. and F.S. designed the study; M.F., W.S., G.M. and T.G. collected and provided sample material; M.R. and J.H. performed laboratory experiments; M.R., J.H., F.S., M.B., W.S., W.G., T.G. and H.G. collected and analysed data; and M.R., G.M. and F.S. wrote the manuscript.

Competing interests

The authors declare no competing interests.

Additional information

Supplementary information The online version contains supplementary material available at https://doi.org/10.1038/s41561-023-01198-z.

Correspondence and requests for materials should be addressed to Manuel Ruben or Gesine Mollenhauer.

Peer review information *Nature Geoscience* thanks Jordon Hemingway and the other, anonymous, reviewer(s) for their contribution to the peer review of this work. Primary Handling Editors: James Super and Rebecca Neely, in collaboration with the *Nature Geoscience* team.

Reprints and permissions information is available at www.nature.com/reprints.